

## BROKEN AND UNBROKEN: THE MILKY WAY AND M31 STELLAR HALOES

A.J. DEASON<sup>1,2,3</sup>, V. BELOKUROV<sup>3</sup>, N.W. EVANS<sup>3</sup>, K.V. JOHNSTON<sup>4</sup>

(Dated: July 24, 2018)  
Draft version July 24, 2018

### ABSTRACT

We use the Bullock & Johnston (2005) suite of simulations to study the density profiles of  $L^*$ -type galaxy stellar haloes. Observations of the Milky Way and M31 stellar haloes show contrasting results: the Milky Way has a ‘broken’ profile, where the density falls off more rapidly beyond  $\sim 25$  kpc, while M31 has a smooth profile out to 100 kpc with no obvious break. Simulated stellar haloes, built solely by the accretion of dwarf galaxies, also exhibit this behavior: some haloes have breaks, while others don’t. The presence or absence of a break in the stellar halo profile can be related to the accretion history of the galaxy. We find that a break radius is strongly related to the build up of stars at apocentres. We relate these findings to observations, and find that the ‘break’ in the Milky Way density profile is likely associated with a relatively early ( $\sim 6 - 9$  Gyr ago) and massive accretion event. In contrast, the absence of a break in the M31 stellar halo profile suggests that its accreted satellites have a wide range of apocentres. Hence, it is likely that M31 has had a much more prolonged accretion history than the Milky Way.

### 1. INTRODUCTION

A diffuse envelope of stars surrounds the Milky Way Galaxy. This halo of stars only contributes a meager few percent to the total light, but comprises the oldest, and most metal-poor stars in the Galaxy. The dynamical timescales in the radial range of the halo stars ( $\sim 10 - 100$  kpc) are long, so these stars can preserve their initial conditions. It is widely recognized that by studying the phase-space and chemical properties of the stellar halo we have the opportunity to unravel the accretion history of our Galaxy.

The density profile of the Milky Way stellar halo has been studied extensively over the past decade. Early work extending out to  $25 - 30$  kpc found that the halo follows an oblate, single power-law distribution with minor-to-major axis ratio  $q \sim 0.5 - 0.8$ , and power-law index  $\alpha \sim 2 - 4$  (e.g. Yanny et al. 2000; Newberg & Yanny 2006; Jurić et al. 2008). More recent work probing further out in the stellar halo has found that the stellar density falls-off more rapidly beyond  $\sim 25 - 30$  kpc with a power-law index of  $\alpha_{\text{out}} \sim 4 - 5$  beyond the break radius (e.g. Watkins et al. 2009; Deason et al. 2011b; Sesar et al. 2011). One could argue that the density distribution can just as easily be described by an Einasto profile (Einasto & Haud 1989), which allows for a steeper fall-off at larger radii, without resorting to a break. However, whether a broken power-law or Einasto profile are preferred, in both cases there exists a characteristic scale (break radius or effective radius) which deserves a physical justification. Is a break radius a ubiquitous feature of stellar haloes? Unfortunately, the low surface brightness of stellar haloes inhibits the study of individual galaxies beyond the local group. However, our nearest neighbor, M31, provides a useful comparison.

Early studies called into question whether a stellar halo even exists in M31: out to  $R \sim 30$  kpc the stellar density profile seems to be a continuation of the M31 bulge (e.g.

Pritchett & van den Bergh 1994; Durrell et al. 2004). However, more recent work extending to larger projected distances (out to  $R \sim 100 - 200$  kpc) does indeed find evidence for a metal-poor halo component with a power-law index of  $\alpha \sim 3.3$  (e.g. Guhathakurta et al. 2005; Irwin et al. 2005; Ibata et al. 2007; Courteau et al. 2011; Gilbert et al. 2012). However, there is no evidence for a break in the M31 stellar halo profile: the density profile follows a continuous single power-law all the way from  $R \sim 30$  kpc to at least  $R \sim 90$  kpc.

Of course, any measure of the smooth, underlying stellar halo density profile (if indeed, it does exist), is hampered by the presence of substructure. A wealth of substructure has now been discovered in both the Milky Way (e.g. Ibata et al. 1995; Newberg et al. 2002; Belokurov et al. 2006; Jurić et al. 2008; Belokurov et al. 2007) and M31 (e.g. Ibata et al. 2001; Ferguson et al. 2002; Gilbert et al. 2007; McConnachie et al. 2009). These discoveries have strongly affirmed the theoretical predictions from numerical simulations that the majority of the stellar halo is built up from the accretion products of satellite galaxies.

Numerical simulations of stellar haloes have developed substantially over the past few years. Bullock & Johnston (2005), hereafter BJ05, presented a suite of 11 stellar haloes built entirely from the disrupted or accreted satellites. More recently, Cooper et al. (2010) used the Aquarius simulations and a dark matter particle ‘tagging’ method to produce stellar haloes in a fully cosmological context. Bell et al. (2008) studied the ‘lumpiness’ of main sequence turn-off (MSTO) stars in the Milky Way stellar halo, and found consistency with the Bullock & Johnston (2005) simulations. This led the authors to suggest that the Milky Way stellar halo is consistent with being built up entirely by accretion. However, Xue et al. (2011) and Deason et al. (2011b) find a somewhat ‘smoother’ stellar halo when traced by blue horizontal branch (BHB) stars. These observations perhaps suggest accretion may not be the only formation mechanism of the stellar halo. Recent hydrodynamic cosmological simulations postulate that some fraction of the inner stellar halo is made up of stars formed *in situ* (e.g. Zolotov et al. 2009; Font et al. 2011). However, stars can diffuse relatively quickly in configuration space (as

<sup>1</sup> Department of Astronomy and Astrophysics, University of California Santa Cruz, Santa Cruz, CA 95064, USA; alis@ucolick.org

<sup>2</sup> Hubble Fellow

<sup>3</sup> Institute of Astronomy, Madingley Rd, Cambridge, CB3 0HA, UK

<sup>4</sup> Department of Astronomy, Columbia University, New York, NY 10027, USA

opposed to velocity space), so the *spatial* structure of the stellar halo can be smooth, even if it is built up from merging and accretion. Thus, a relatively smooth stellar halo could also signify an early accretion history.

In this paper we study the density profiles of stellar haloes drawn from the BJ05 suite of simulations. We investigate the origin of ‘broken’ density profiles, and in particular, address why some haloes have an obvious break (e.g. the Milky Way) and why some do not (e.g. M31). We know that accretion is at least an important (if not the sole) contributor to the stellar halo. By comparison with the BJ05 simulations we hope to link the observed stellar halo profiles of local galaxies to their accretion histories.

The paper is arranged as follows. In Section 2 we briefly describe the BJ05 simulations. In Section 3 we study the stellar halo density profiles of the 11 haloes drawn from the BJ05 simulations. In Section 4 we investigate the origin of broken halo profiles and we discuss the implications for the Milky Way and M31 stellar haloes in Section 5. Finally, we summarize our main findings in Section 6.

## 2. BULLOCK AND JOHNSTON SIMULATIONS

The Bullock & Johnston simulations (see BJ05 for full details), are a suite of 11 high resolution stellar haloes built up from the accretion of dwarf galaxies onto a Milky Way-like potential. The parent galaxy is represented by a time-dependent, analytical potential consisting of bulge, disk and halo components. The accretion history of each halo is randomly drawn within the context of a  $\Lambda$ CDM Universe; each accretion event was assigned a binding energy and orbital eccentricity drawn from the orbital distributions of satellites observed in cosmological simulations of structure formation. High resolution N-body simulations were then run to track the evolution of dark matter particles in each accretion event. At the present day ( $z = 0$ ), individual haloes are built up from the disruption of  $N > 100$  dwarf galaxies.

The baryonic component of each dwarf galaxy is followed by assuming that the cold gas inflow tracks the dark matter accretion rate<sup>5</sup>. The gas mass is then used to determine the instantaneous star formation rate and to track the buildup of stars within each halo. The stellar matter in each dwarf galaxy is associated with the most tightly bound material in the halo. Variable mass-to-light ( $M/L$ ) ratios for each particle are assigned in order to produce realistic dwarf galaxy stellar profiles; the  $M/L$  is chosen so that the luminous matter in the infalling satellites initially follows a King model embedded within an Navarro-Frenk-White (NFW) dark matter potential. The King profiles were chosen to specifically reproduce structure (e.g. sigma vs. core relations) observed for dwarf satellites today. The time dependent chemical content of the dwarf galaxies is also included in the models (see Robertson et al. 2005 and Font et al. 2006 for more details). The stellar population models include enrichment from Type Ia and Type II supernova, as well as stellar winds. A physically motivated supernova feedback prescription is used to reproduce the local dwarf galaxy stellar mass-metallicity relation. The rate of chemical enrichment is calculated analytically, and the abundances of H, He, Fe, and the  $\alpha$ -elements O and Mg are tracked in the simulations.

BJ05 verified that their models are able to reproduce a number of observational constraints, such as the number and

<sup>5</sup> This assumption holds prior to infall into the parent halo; the star formation is truncated soon after each satellite is accreted.

ID(BJ05)	SPL- $\alpha$	BPL- $\alpha_{in}$	BPL- $\alpha_{out}$	BPL- $r_b$ [kpc]	$P_{KS}$
02(1)	3.4	2.0	4.5	26	0.071
05(2)	3.2	2.7	4.6	38	0.020
07(3)	3.6	2.3	5.0	24	0.007
08(4)	2.5	2.7	2.5	22	1.000
09(5)	3.2	2.8	5.1	38	0.001
10(6)	3.0	2.7	6.5	60	0.020
12(7)	3.0	2.0	3.4	21	0.939
14(8)	3.2	2.1	3.6	25	0.985
15(9)	2.9	2.4	3.1	23	0.853
17(10)	2.9	1.6	5.6	43	0.031
20(11)	3.1	2.1	4.4	30	0.207

**Table 1**

The global properties of the 11 BJ05 stellar haloes. We give the halo ID from galaxia (see <http://galaxia.sourceforge.net/>) and BJ05 in parenthesis, the best-fit single power-law slope, the best-fit broken power-law slopes and break radii and the KS test (SPL versus BPL) probability.

distribution of structural parameters of the Milky Way’s satellite population. Furthermore, the resulting stellar haloes have a similar luminosity ( $\sim 10^9 L_{\odot}$ ) and density profile to the Milky Way ( $\alpha \sim 3.5$ ), and contain a similar amount of substructure (Bell et al. 2008). The scatter between the 11 simulated stellar haloes is due to their different accretion histories; we will explore the effect of accretion history on the stellar halo density profiles in the following sections.

## 3. STELLAR HALO DENSITY PROFILE

We investigate the density profile of halo stars belonging to the eleven parent haloes discussed in BJ05. Table 1 in BJ05 shows that the majority (80-90 %) of the stellar halo is built up from the 15 most massive accreted satellites. For this reason, we only consider the contribution to the stellar halo from the 15 largest satellites. We fit single power-law (SPL) and broken power-law (BPL) density profiles to stellar haloes between 10-100 kpc. To fit the density profiles, we compute the density in radial bins and use the MPFIT IDL routine (Markwardt 2009) to find the minimum Chi-square SPL or BPL density profile. The best-fit parameters for the density profiles are given in Table 1. In addition, we also fit profiles for stars belonging to *individual* accretion events. Provided the accretion event is not too recent (less than 4.5 Gyr ago, cf. Figure 3 in Johnston et al. 2008), a BPL is a good description of the density profile (see e.g. Fig. 3).

The density profile for each stellar halo is shown by the thick black lines in Fig. 1. The dashed blue line shows the best-fit BPL profile for the stellar halo, and the break radius for this fit is shown by the vertical dotted line. The thinner lines show the profiles for the 5 most massive accreted satellites. The fraction (by mass) contributed to the stellar halo (between 10-100 kpc) decreases from thicker black lines to thinner red lines.

Fig. 1 shows that a broken power-law profile is generally a good description of the stellar halo density profiles, where the

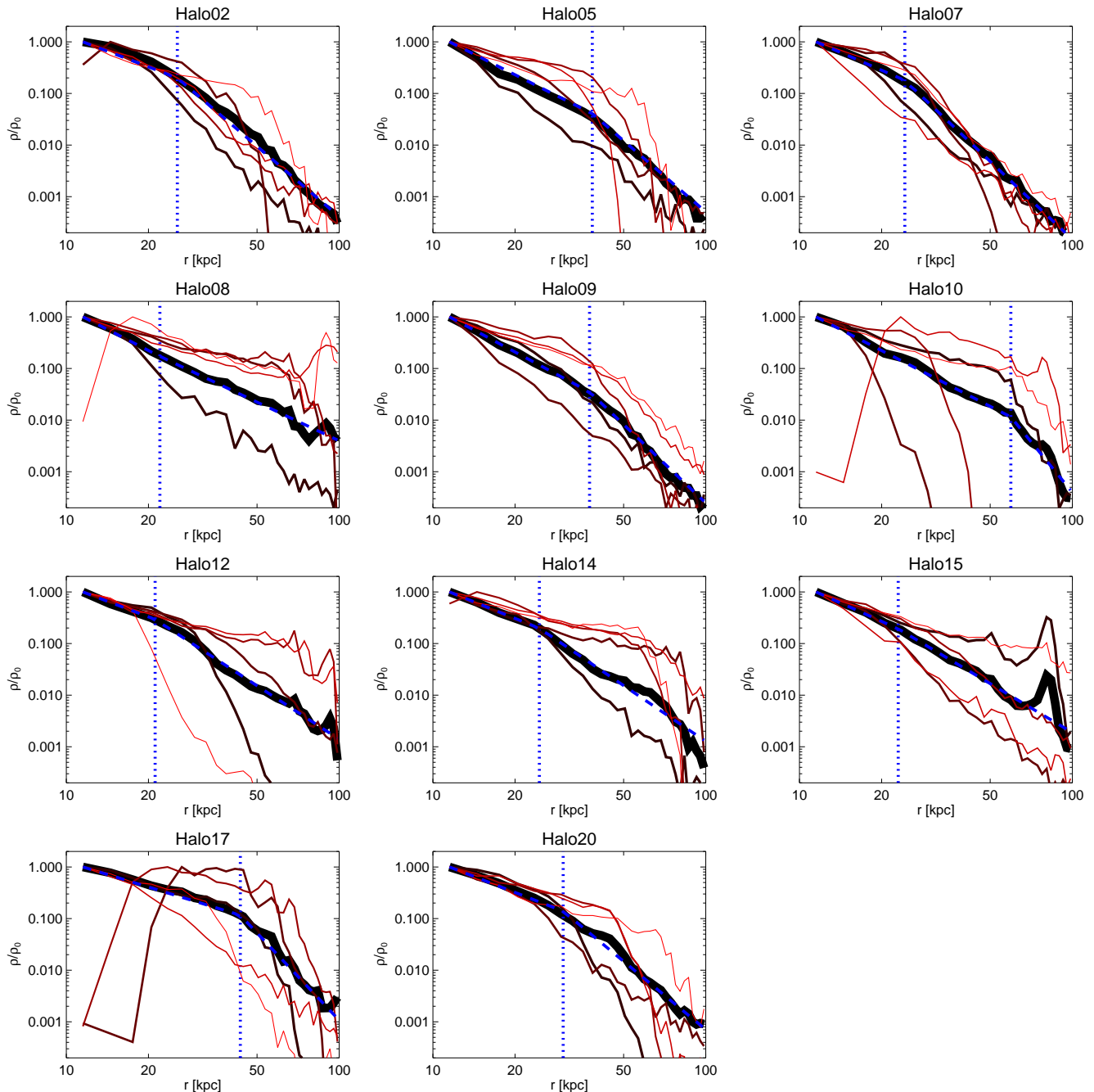


**Figure 1.** Radial density profiles of the 11 BJ05 stellar haloes. The thick black line shows the overall profile for the 15 most massive satellites that contribute to the stellar halo within 100 kpc. The thinner lines show the profiles for the 5 most massive accreted subhaloes. The fraction (by mass) contributed to the stellar halo decreases from thicker black to thinner red lines. The blue dashed line shows the best-fit BPL profile for the stellar halo, and the vertical dotted line indicates the corresponding break-radius.

stellar density falls off more rapidly beyond the break radius. Such ‘broken’ stellar haloes are also seen in the stellar haloes of Cooper et al. (2010) (see also BJ05). However, it is worth noting that some stellar haloes can just as easily be described by a single power-law.

#### 4. ORIGIN OF BROKEN PROFILES

The stellar halo in the BJ05 models is a superposition of stars stripped from several satellite galaxies. Thus, to understand the origin of the global stellar halo profile, we must first investigate the profiles of stars belonging to individual accretion events. The density profile of stars stripped from an in-

dividual satellite galaxy is well-described by a BPL (see e.g. Fig. 3). What causes this BPL profile?

For each star particle, we find the apocentre and pericentre of its orbit. Assuming a spherically symmetric, stationary potential, we can estimate the apocentre and pericentre from the following equation (see Binney & Tremaine 1987, Chapter 3):

$$u^2 + \frac{2[\Phi(1/u) - E]}{L^2} = 0. \quad (1)$$

Here,  $u = 1/r$  and the roots of this equation give the apocentre and pericentre. This equation can be solved for each star

particle given the potential and particle properties defined at redshift  $z = 0$ . This is a good approximation to the orbital properties of the stars at the *time of stripping*. However, the orbital properties may have evolved since the time of accretion onto the parent halo. In Appendix A, we verify some of our deductions made from the halo star properties at redshift  $z = 0$  by tracing back the orbital histories of the accreted satellites.

From the inferred orbital properties of the stars, we can find the average apocentre and pericentre of the stars belonging to an individual satellite accretion event. As the star particles can have different masses (see BJ05 for details), we compute the mass weighted average. In the top panel of Fig. 2, we show the average apocentre of star particles belonging to one satellite against the best-fit break radius for the density profile of these stars. The satellites from all eleven parent haloes are shown in this plot. We also show the average properties for the global stellar haloes with the star symbols. There is a clear correlation between apocentre and break radius; here, the dotted line indicates a one-to-one relation.

The colors in the top panel of Fig. 2 indicate the *strength* of the break. To characterize the break strength we perform a two-sided KS test on the best-fit SPL and BPL density models. Weak breaks will have a high probability of being drawn from the same distribution as the SPL profile (i.e.  $P_{KS} \sim 1$ ), while strong breaks will have a low probability (i.e.  $P_{KS} \sim 0$ ). One can see that the points deviating the most from a one-to-one relation between apocentre and break radius tend to have the weakest breaks.

The bottom panel of Fig. 2 shows the average time of (stellar) stripping for each satellite ( $T_{ub}$ , in Gyr) against the average apocentre at  $z = 0$ . Satellites accreted at early times have smaller apocentres as the physical size (and mass) of the parent galaxy is smaller. Therefore, breaks give an indication of *when* a satellite was accreted and/or disrupted. However, a further complication is dynamical friction, as more massive satellites can sink to the center of the parent halo relatively quickly. The colors in the bottom panel of Fig. 2 indicate the satellite (stellar) mass. More massive satellites tend to have smaller apocentres (at stripping) even if they are accreted relatively recently.

In Fig. 3, we show the radial velocity structure of three accreted satellites in Halo05. The stripped material from the satellite in the left-hand panel shows an obvious break in the density profile which coincides with the apocentres of its star particle orbits. The middle panel shows a (massive) satellite accreted a long time ago ( $\sim 9$  Gyr ago) which is now well mixed in phase-space and can be described by a single power-law density profile (cf. Johnston et al. 2008). Finally, the right-hand panel illustrates a relatively recent accretion remnant for which the density profile is poorly defined. In general, satellites accreted between 4.5-9 Gyr ago follow a BPL density profile. Satellites accreted a long time ago ( $T_{ub} \gtrsim 9$  Gyr), can be well mixed in phase-space, and recent accretion events ( $T_{ub} \lesssim 4.5$  Gyr ago) are unrelaxed and their density profiles are poorly defined.

We have found that the satellite apocentre sets the scale of the break radius, but what sets the ‘strength’ of the break? In the top panel of Fig. 4 we show the break strength (defined by a two-sided KS test between SPL and BPL profiles) against the spread of apocentres for stars belonging to an individual satellite. We find that stronger breaks have a smaller spread in particle apocentres. The spread in apocentres is related to the energy distribution of the star particles; the bottom left-

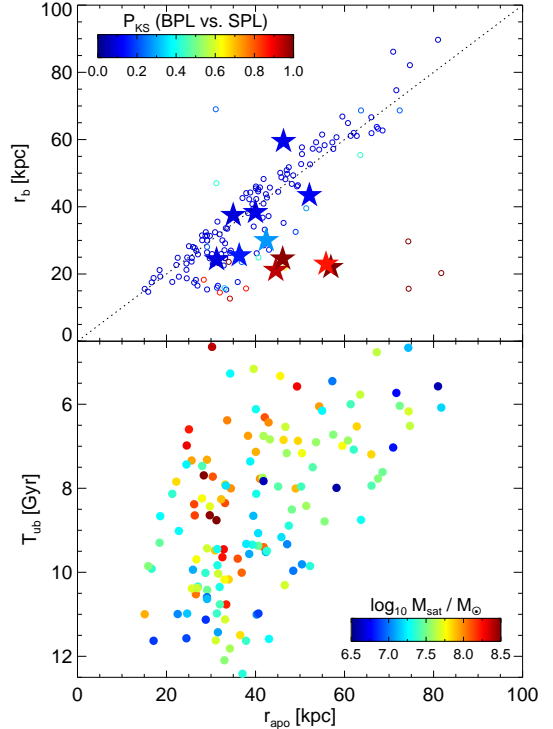


**Figure 2.** *Top panel:* The break radius of the stellar density profile against the average apocentre of the star particle orbits. The circle symbols indicate individual accreted satellite remnants from all 11 stellar haloes, and the star symbols indicate their global values. The colors indicate the probability that the best-fit single power-law density profile is drawn from the same distribution as the best-fit broken power-law density profile (i.e. using a two-sided KS test). The red colors indicate profiles which do not have a strong break in the stellar halo density. The dotted line shows a one-to-one relation. *Bottom panel:* The average time of stripping for each accreted satellite against the apocentre of the orbits. Satellites accreted at early times have smaller apocentres as the physical size (and mass) of the parent galaxy is smaller. The colors indicate the satellite (stellar) mass. More massive satellites are more affected by dynamical friction, so can sink to the center of their parent halo more quickly than less massive satellites.

hand panel of Fig. 4 shows that the dispersion in energy of an accreted remnant is strongly correlated with the spread in particle apocentres. Note that these relations also hold for the global stellar halo properties (shown by the blue star symbols). Here, the spread in apocentre is calculated from all 15 satellite accretion remnants.

The bottom right-hand panel of Fig. 4 shows that more massive satellites have a larger spread in energy (as expected analytically, see e.g. Johnston 1998). The colors indicate the average time of stripping for each satellite. Satellites accreted a long time ago ( $T_{ub} \gtrsim 9$  Gyr) can have a large spread in energy, regardless of the satellite mass (cf. phase-mixed example in middle-panel of Fig. 3).

## 5. IMPLICATIONS FOR GLOBAL STELLAR HALO PROPERTIES

In the previous section, we found that the density profile of stars stripped from an individual satellite is strongly related to the orbital structure of the stars. The average apocentre of the star particle orbits corresponds to the break radius of the best-fit BPL density profile. Furthermore, the strength of the break depends on the spread in energy (and hence apocentres)

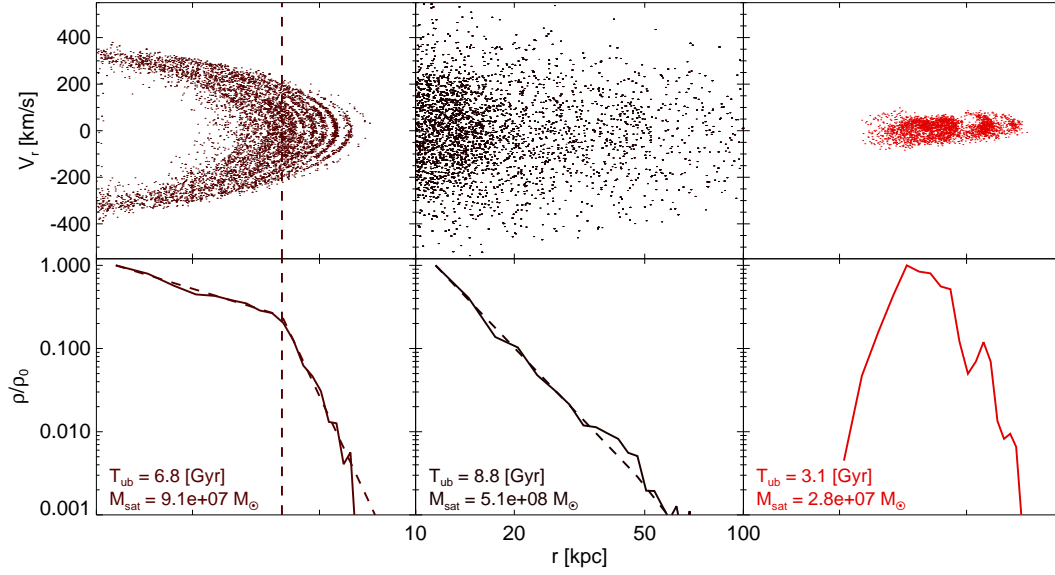


**Figure 3.** Examples of individual satellite contributions to the global stellar halo. Three satellites accreted/disrupted at different times in Halo05 are shown. The top panels show their radial velocities as a function of radius and the bottom panels show their density profiles. The dashed-line is the best-fit broken power-law model. In the left-hand panel, there is an obvious ‘break’ in the stellar density which coincides with the average apocentre of the star particle orbits. Satellites disrupted a long time ago ( $T_{ub} \gtrsim 9$  Gyr) are often well phase-mixed and follow a single power-law profile. Recent accretion events ( $T_{ub} \lesssim 4.5$  Gyr) are often unrelaxed and have poorly defined (i.e. non-smooth) density profiles.

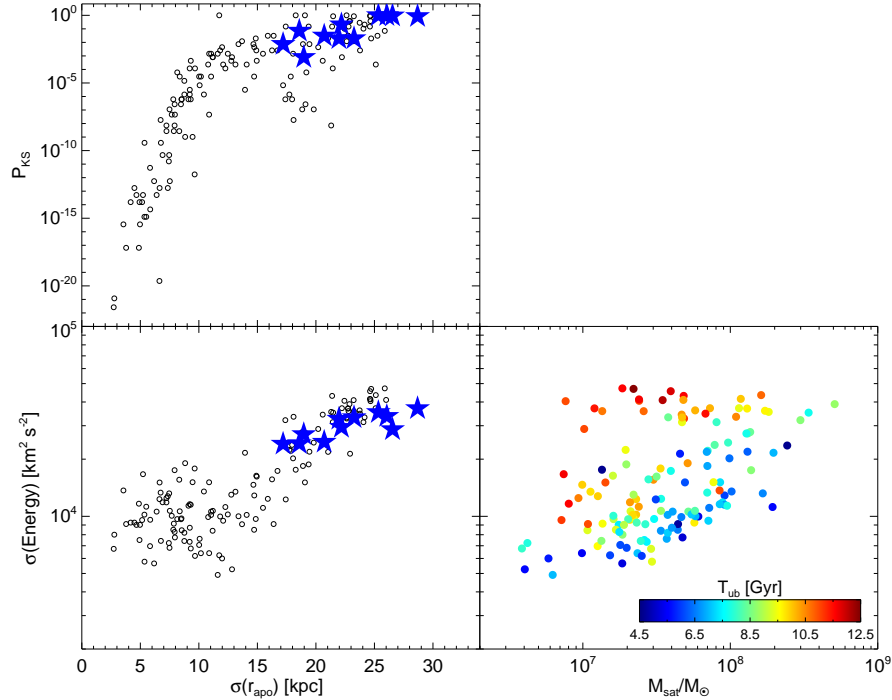


**Figure 4.** *Top panel:* The ‘strength’ of the broken power-law density model against the dispersion of star particle apocentres. The strength of the break is characterized by a KS test between single and broken power-law density models. A high probability that the best-fit single power-law model is drawn from the same distribution as the best-fit broken power-law model indicates a weak, if not non-existent, break in the stellar density profile. The black circles are individual satellites and the blue stars indicate the global stellar halo properties. *Bottom-left panel:* The dispersion in energy of star particles against the dispersion in star particle apocentres. A large range of star particle energies leads to a large dispersion in their apocentres, and hence a weaker break in the stellar density profile. *Bottom-right panel:* The dispersion in energy of star particles against satellite mass. Higher mass satellites have a larger range of particle energies. The colors indicate the time of stripping.

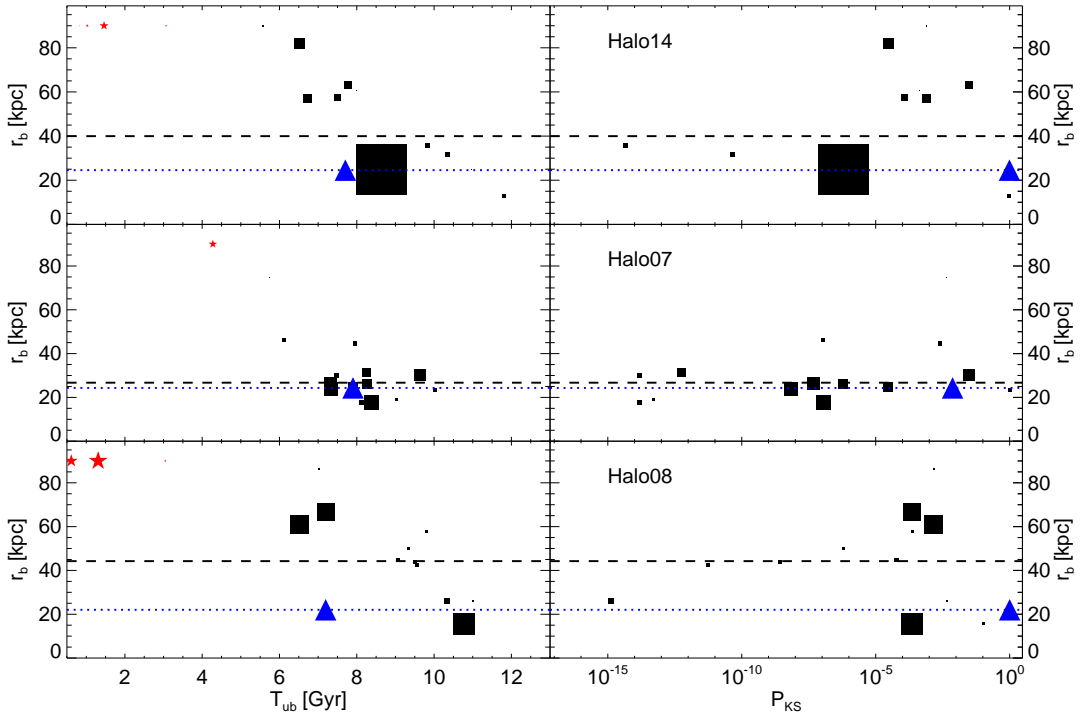


**Figure 5.** Examples of three stellar haloes. The black squares show the break radii of the 15 most massive accretion events against disruption time (left panels) and strength of break (right panels). The sizes of the square symbols indicate the fractional contribution of each satellite to the overall stellar halo (larger squares are more massive satellites). The blue dotted line and blue triangles indicate the overall stellar halo properties. The red stars indicate recent accretion events ( $T_{\text{ub}} \lesssim 4.5$  Gyr) where the density profiles of the remnants are poorly defined. These are placed at  $r_b = 90$  kpc for illustrative purposes. The dashed black line indicates the *mass-weighted* break radius. This is calculated by computing the weighted mean of all 15 satellites’ break radii. Haloes 14 and 07 (top and middle panels) can both be described by a broken power-law stellar density profile (albeit Halo14 has a relatively weak break:  $P_{\text{KS}} \sim 0.99$  and  $\alpha_2 - \alpha_1 = 1.5$ ). In the latter case the accreted satellites all have similar apocentres (and hence break-radii) whereas the former halo is dominated by one massive satellite. Halo08 (bottom panel) has no obvious break ( $P_{\text{KS}} \sim 1$  and  $\alpha_2 - \alpha_1 = -0.2$ ) and its accreted satellites have a wide range of apocentres.

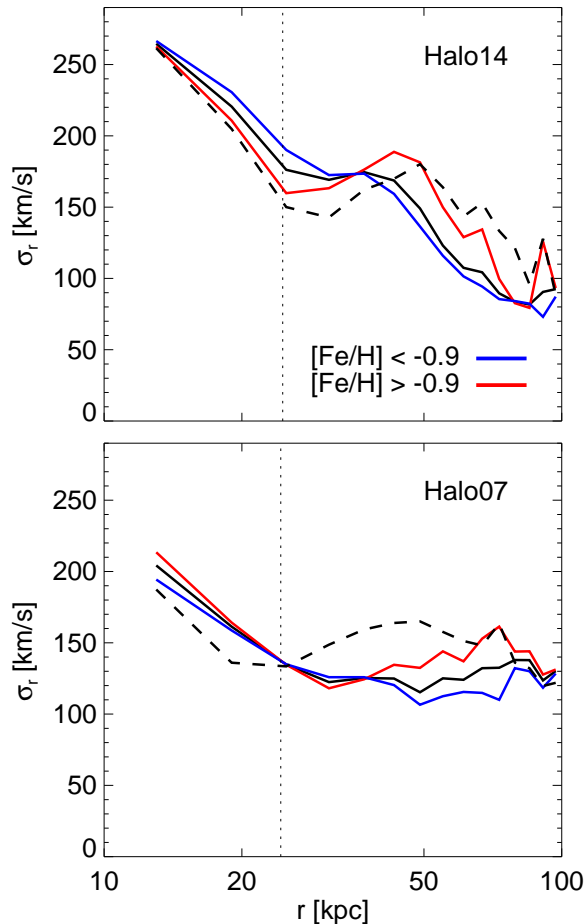


**Figure 6.** Radial velocity dispersion profile for two example haloes. The black lines show the overall profiles, the red/blue lines show the profiles for star particles with metallicity greater than/less than  $[\text{Fe}/\text{H}] = -0.9$ . The dashed lines show the profiles for the stars belonging to the most massive satellite accreted by the galaxy. The dotted lines indicate the break radii of each halo. The stellar halo of Halo14 is dominated by one massive satellite whilst Halo07 is built up from several similar mass satellites with similar apocentres. The metal-rich(er) velocity dispersion profile for Halo14 shows a more pronounced ‘dip’ near the break radius. There is little difference between the metal-rich(er) and metal-poor(er) profiles for Halo07, indicating that the break is not dominated by a single, massive accretion event.

of the stars. In general, more massive satellites have a larger energy spread. However, very early accretion events ( $T_{\text{ub}} \gtrsim 9$  Gyr ago) which are well mixed in phase-space can also have a large spread in energy, regardless of the initial satellite mass.

We now relate these findings to the global stellar halo properties. The global stellar halo is a superposition of individual satellite contributions. Therefore, the overall stellar density break radius reflects the individual satellite contributions. For example, a strong break ensues when the accreted satellites all have similar apocentres (e.g. Halo07, middle panel of Fig. 5). The halo can also be dominated by one massive satellite (e.g. Halo14, top panel of Fig. 5), and the overall break radius reflects the apocentre of this massive satellite. In Fig. 5 we show the best-fitting break radius for individual satellite contributions versus average time of stripping (left-hand column) and strength of break (right-hand column). The size of the black squares illustrates the satellite mass (larger symbols

for more massive satellites). The blue triangles indicate the global parent stellar halo properties and the blue dotted line indicates the parent stellar halo break radius. We also show the ‘mass-weighted’ global break radius by the black-dashed line. This is computed from the individual satellite break radii weighted by their mass. The top two rows illustrate the two different scenarios mentioned above. In Halo14 the overall stellar halo density profile is dominated by one massive satellite, whilst in Halo07 several satellites (of comparable) mass have very similar break radii.

Are we able to discern between these two scenarios? Fig. 6 shows the radial velocity dispersion profiles for these two haloes. The black line is the overall profile, and the red and blue colors illustrate the profiles for metal-rich(er) and metal-poor(er) stars (arbitrarily split at the average metallicity of the stellar haloes  $[\text{Fe}/\text{H}] = -0.9$ ). The profile for the most massive satellite contributing to the stellar halo (between 10–100 kpc) is shown by the black dashed line. In both Halo07 and Halo14 there are ‘dips’ in the velocity dispersion profile near the break radius (indicated by the vertical dotted line). This is a result of the low radial velocities of the star particles at the apocentres of their orbits. However, in Halo14 this dip is much more pronounced in the higher-metallicity stars. This is because a massive satellite, which is therefore relatively metal-rich, dominates the break in Halo14. One can see that the profile for this massive satellite (dashed black line) closely follows the profile for the most metal-rich stars in the halo. There is little difference between the metal-rich and metal-poor material in Halo07. This is because all of the satellites in Halo07 (low and high mass) have very similar apocentres, and there is no massive, dominating accretion remnant.

Finally, we consider the case where there is no obvious break in the stellar density profile. In this case, the accretion events may have a wide range of apocentres (e.g. Halo08, bottom row of Fig. 5). As the apocentre is related to the time of accretion, this suggests that the accretion history has been prolonged. The bottom row of Fig. 5 shows that there have been significant satellite disruption events over a wide time interval: from  $\sim 11$  Gyr ago to recent events only  $\sim 1$  Gyr ago. In comparison, Halo14 and Halo07 show little activity in the last 6 Gyr.

In summary, the stellar halo density profile, and in particular the presence or absence of a break in the stellar density, can give us an important insight into the accretion history of a galaxy.

### 5.1. The Milky Way and M31

In the last few years, several groups have found that the Milky Way stellar halo has a ‘broken’ density profile (e.g. Bell et al. 2008; Sesar et al. 2011; Deason et al. 2011b), with  $r_b = 20 - 30$  kpc and  $\alpha_{\text{in}} = 2.3 - 2.8$  and  $\alpha_{\text{out}} = 3.8 - 4.6$ . Furthermore, Deason et al. (2011a) found a dip in the line-of-sight<sup>6</sup> velocity dispersion profile of the *metal-rich(er)* ( $[\text{Fe}/\text{H}] > -2$ ) blue horizontal branch stars (see Figure 6 in Deason et al. 2011a). This dip in velocity dispersion occurs between 20–30 kpc, in the approximate radial range where there is a break in the stellar density profile.

Our conclusions in the previous sections suggest that these observations may have several important implications:

- The relatively close-by break radius of the Milky Way

<sup>6</sup> In the radial range of the Deason et al. (2011a) study, 10–50 kpc, the line-of-sight velocity is a good approximation for the radial velocity

( $r_b = 20\text{--}30$  kpc) is likely caused by accreted satellites with small apocentres (at the time of stripping).

- The cold velocity dispersion profile near the break radius provides further evidence for the break-apocentre connection.
- A metal-rich bias in the velocity dispersion profile suggests that the break in the Milky Way stellar halo could be dominated by a (relatively) *massive* satellite(s).
- The density profile has only been measured out to 50 kpc, so we cannot rule out more recent accretion events with larger apocentres. However, the relatively smooth stellar density profile out to 50 kpc (Deason et al. 2011b) suggests *early* accretion events and then somewhat quiescent evolution.

Recently, Gilbert et al. (2012) measured the density profile of the M31 stellar halo out to 100 kpc (see also earlier work by Guhathakurta et al. 2005, Irwin et al. 2005, Ibata et al. 2007 and Courteau et al. 2011). These authors find that the stellar distribution can be described by a SPL with  $\alpha \sim 3.3$ , and there is no evidence for a break in the density profile. As we found in the previous section, no obvious break in the global stellar halo profile indicates that the stars have a wide range of apocentres, which suggests that M31 has had a much more prolonged accretion history than the Milky Way (see e.g. Halo08). This deduction, that M31 appears to have experienced a much more active accretion history than the Milky Way, is in good agreement with other independent observations of the two galaxies: Relative to the Milky Way, M31 has a more disturbed disc (e.g. Brown et al. 2006), a larger bulge (e.g. Pritchett & van den Bergh 1994; Durrell et al. 2004), a younger and more metal-rich halo population (e.g. Irwin et al. 2005; Kalirai et al. 2006), and more numerous tidal streams and surviving satellite galaxies (e.g. Koch et al. 2008; Richardson et al. 2011).

## 6. CONCLUSIONS

The stellar haloes of the Milky Way and M31 have conflicting density profiles: the Milky Way has a broken profile, whereby the stellar density falls off more rapidly beyond a break radius ( $r_b \sim 25$  kpc), whereas, the stellar halo of M31 shows no obvious break and can be described by a single power-law. In light of these recent observations, we have studied the density profiles of stellar haloes – built solely by the accretion of dwarf galaxies – drawn from the Bullock & Johnston (2005) suite of simulations, with the aim of understanding the contrasting stellar haloes of our local galaxies.

We summarize our conclusions as follows:

- (1) The simulated haloes often have ‘broken’ stellar halo profiles, where the density falls off more quickly beyond the break radius. However, some haloes do not have an obvious break, and their density distribution can be described by a single power-law (e.g. the Milky Way versus M31).
- (2) In the BJ05 simulations, the global stellar halo is a superposition of accretion products from the  $\sim 15$  massive accretion events. The density profiles of the stars that once belonged to an individual satellite follow a broken profile, where the break radius corresponds to the average apocentre of the

stars. However, material belonging to recently stripped satellites ( $T_{\text{ub}} \lesssim 4.5$  Gyr) have ill-defined density profiles, and very ancient accretion events ( $T_{\text{ub}} \gtrsim 9$  Gyr) are often well-mixed in phase-space.

- (3) The location of the break in the stellar density is linked to the time of accretion/stripping and the mass of the satellite. Satellites accreted at early times have smaller apocentres as the physical size of the parent halo is smaller. More massive satellites can have smaller apocentres (and hence break radii) at the time of stripping, as the satellite can spiral into the center of the galaxy via dynamical friction.

- (4) The strength of the break in the stellar density depends on the spread of apocentres of the stars. For the global stellar halo, the break strength depends on the range of apocentres of its accreted components. Individual satellite accretion remnants can also have varying break strengths. More massive satellites have a larger spread in energy (and hence apocentres). Also, stars belonging to satellites accreted a long time ago can have a wide spread in energy as they are well mixed in phase-space today.

- (5) The global stellar halo density profile depends on the accretion history of the galaxy. An obvious break in the overall density profile suggests that: (a) the accreted satellites have similar apocentres; or (b) one massive satellite dominates the stellar density in the applicable radial range. These two scenarios could be distinguished observationally. The radial velocities of stars near apocentre are very low, thus the radial velocity dispersion is also low (i.e. shell-type structures). In case (b) above, the apocentres of stars that once belonged to a massive, and hence metal-rich, satellite dominate the break. Thus, a ‘dip’ in the velocity dispersion profile, the signature of a build-up of apocentres, will be more pronounced in the *metal-rich(er)* material. Conversely, if the accreted satellites all have similar masses (and similar apocentres), then we would expect no metallicity bias.

- (6) The profiles of some haloes show no obvious break in the stellar density. Often, these haloes have a prolonged accretion history whereby satellites are accreted over a wide range of timescales ( $\sim 0\text{--}10$  Gyr ago). Thus, the average apocentres of the accreted satellites, whose material now makes up the stellar halo, also have a wide range of values.

Our investigation into the simulated BJ05 stellar haloes has provided some important insights into the accretion histories of the Milky Way and M31. The absence of a break in the M31 stellar halo suggests that this galaxy has had a prolonged accretion history, where the accreted satellites had a wide range of apocentres. However, the strong break in the Milky Way stellar halo (at  $r_b = 20\text{--}30$  kpc), in addition to the presence of a shell-type feature in the relatively metal-rich BHB stars, suggests that the stellar halo break is dominated by the apocentre of a (relatively) massive satellite.

## ACKNOWLEDGMENTS

We thank an anonymous referee for valuable comments. AJD is currently supported by NASA through Hubble Fellowship grant HST-HF-51302.01, awarded by the Space Telescope Science Institute, which is operated by the Association of Universities for Research in Astronomy, Inc., for NASA, under contract NAS5-26555.

## REFERENCES

- Bell, E. F., et al. 2008, *ApJ*, 680, 295
- Belokurov, V., et al. 2006, *ApJ*, 642, L137
- , 2007, *ApJ*, 657, L89
- Binney, J., & Tremaine, S. 1987, *Galactic dynamics* (Princeton, NJ, Princeton University Press, 1987, 747 p.)
- Brown, T. M., et al. 2006, *ApJ*, 652, 323
- Bullock, J. S., & Johnston, K. V. 2005, *ApJ*, 635, 931
- Cooper, A. P., et al. 2010, *MNRAS*, 406, 744
- Courteau, S., Widrow, L. M., McDonald, M., Guhathakurta, P., Gilbert, K. M., Zhu, Y., Beaton, R. L., & Majewski, S. R. 2011, *ApJ*, 739, 20
- Deason, A. J., Belokurov, V., & Evans, N. W. 2011a, *MNRAS*, 411, 1480
- , 2011b, *MNRAS*, 416, 2903
- Durrell, P. R., Harris, W. E., & Pritchett, C. J. 2004, *AJ*, 128, 260
- Einasto, J., & Haud, U. 1989, *A&A*, 223, 89
- Ferguson, A. M. N., Irwin, M. J., Ibata, R. A., Lewis, G. F., & Tanvir, N. R. 2002, *AJ*, 124, 1452
- Font, A. S., Johnston, K. V., Bullock, J. S., & Robertson, B. E. 2006, *ApJ*, 646, 886
- Font, A. S., McCarthy, I. G., Crain, R. A., Theuns, T., Schaye, J., Wiersma, R. P. C., & Dalla Vecchia, C. 2011, *MNRAS*, 416, 2802
- Gilbert, K. M., et al. 2007, *ApJ*, 668, 245
- , 2012, *ArXiv e-prints*
- Guhathakurta, P., Ostheimer, J. C., Gilbert, K. M., Rich, R. M., Majewski, S. R., Kalirai, J. S., Reitzel, D. B., & Patterson, R. J. 2005, *ArXiv Astrophysics e-prints*
- Ibata, R., Irwin, M., Lewis, G., Ferguson, A. M. N., & Tanvir, N. 2001, *Nature*, 412, 49
- Ibata, R., Martin, N. F., Irwin, M., Chapman, S., Ferguson, A. M. N., Lewis, G. F., & McConnachie, A. W. 2007, *ApJ*, 671, 1591
- Ibata, R. A., Gilmore, G., & Irwin, M. J. 1995, *MNRAS*, 277, 781
- Irwin, M. J., Ferguson, A. M. N., Ibata, R. A., Lewis, G. F., & Tanvir, N. R. 2005, *ApJ*, 628, L105
- Johnston, K. V. 1998, *ApJ*, 495, 297
- Johnston, K. V., Bullock, J. S., Sharma, S., Font, A., Robertson, B. E., & Leitner, S. N. 2008, *ApJ*, 689, 936
- Jurić, M., et al. 2008, *ApJ*, 673, 864
- Kalirai, J. S., et al. 2006, *ApJ*, 648, 389
- Koch, A., et al. 2008, *ApJ*, 689, 958
- Markwardt, C. B. 2009, in *ASP Conf. Ser.*, Vol. 411, *Astronomical Data Analysis Software and Systems XVIII*, ed. D. A. Bohlender, D. Durand, & P. Dowler, 251
- McConnachie, A. W., et al. 2009, *Nature*, 461, 66
- Newberg, H. J., & Yanny, B. 2006, *Journal of Physics Conference Series*, 47, 195
- Newberg, H. J., et al. 2002, *ApJ*, 569, 245
- Pritchett, C. J., & van den Bergh, S. 1994, *AJ*, 107, 1730
- Richardson, J. C., et al. 2011, *ApJ*, 732, 76
- Robertson, B., Bullock, J. S., Font, A. S., Johnston, K. V., & Hernquist, L. 2005, *ApJ*, 632, 872
- Sesar, B., Jurić, M., & Ivezić, Ž. 2011, *ApJ*, 731, 4
- Watkins, L. L., et al. 2009, *MNRAS*, 398, 1757
- Xue, X.-X., et al. 2011, *ApJ*, 738, 79
- Yanny, B., et al. 2000, *ApJ*, 540, 825
- Zolotov, A., Willman, B., Brooks, A. M., Governato, F., Brook, C. B., Hogg, D. W., Quinn, T., & Stinson, G. 2009, *ApJ*, 702, 1058

## APPENDIX

RELATING SATELLITE PROPERTIES AT ACCRETION TO  $Z = 0$  HALO STARS

In this section, we verify some of our deductions from the star particle properties at  $z = 0$ , by tracing back the accreted satellites whose stripped stellar material make up the stellar haloes today.

We follow the orbits of satellites from Halo02 and Halo07. In the left-hand panels of Fig. 7 we show three examples of satellites from Halo07. These are the three most massive contributors to the stellar halo within 100 kpc of this galaxy. In the left columns we show the evolution of radius with time for the satellites, and the right columns show the evolution of total satellite mass with time. The red dashed line indicates the average time when stars become unbound ( $\langle T_{\text{ub}} \rangle$ ) from the satellite. The dotted black line indicates the average apocentre of the star particles computed in Section 4, and the solid blue line indicates the approximate break radius in the density profile of the stripped stellar material. This figure shows that the break radius we measure at  $z = 0$  from the stars is indeed coincident with the apocentre of the host satellite galaxy near the time of stripping. In Section 4, we deduced this by estimating the apocentre of star particle orbits using Equation 1.

In the right-hand panels of Fig. 7 we relate some of the initial satellite properties to those we infer from their stripped stars at  $z = 0$ . The top-left panel of this figure shows the relation between accretion time (of the satellite) and the average time at which the star particles become unbound. The stars are stripped a few Gyr after satellite accretion, but there remains a positive correlation between these two timescales. The bottom-left panel shows that the difference between these timescales is related to the mass of the satellite galaxy. Due to dynamical friction effects, more massive satellites spend a shorter amount of time orbiting the galaxy before the stellar material is stripped. In the top-right panel we show satellite accretion time against initial satellite apocentre (red asterisks) and average star particle apocentres at  $z = 0$  (filled black circles). In Section 4, we noted that larger apocentres correspond to more recent accretion events as the physical size, and mass of the parent galaxy is larger, and hence more distant satellites can be captured. The strong trend between initial apocentre and accretion time reinforces this statement. Although the trend is slightly weaker, we see that the apocentres of the stripped stars at  $z = 0$  are still an indication of when their host satellite was accreted. The final apocentre of the satellite (and hence stripped stars) is generally reduced from the initial apocentre via dynamical friction effects. In the bottom-right panel of the figure we show that the difference in apocentre radius is strongly related to the satellite mass.

In summary, we find that our deductions made from the  $z = 0$  halo stars in the main section of the text, are verified when we trace the accreted satellite properties back in time.

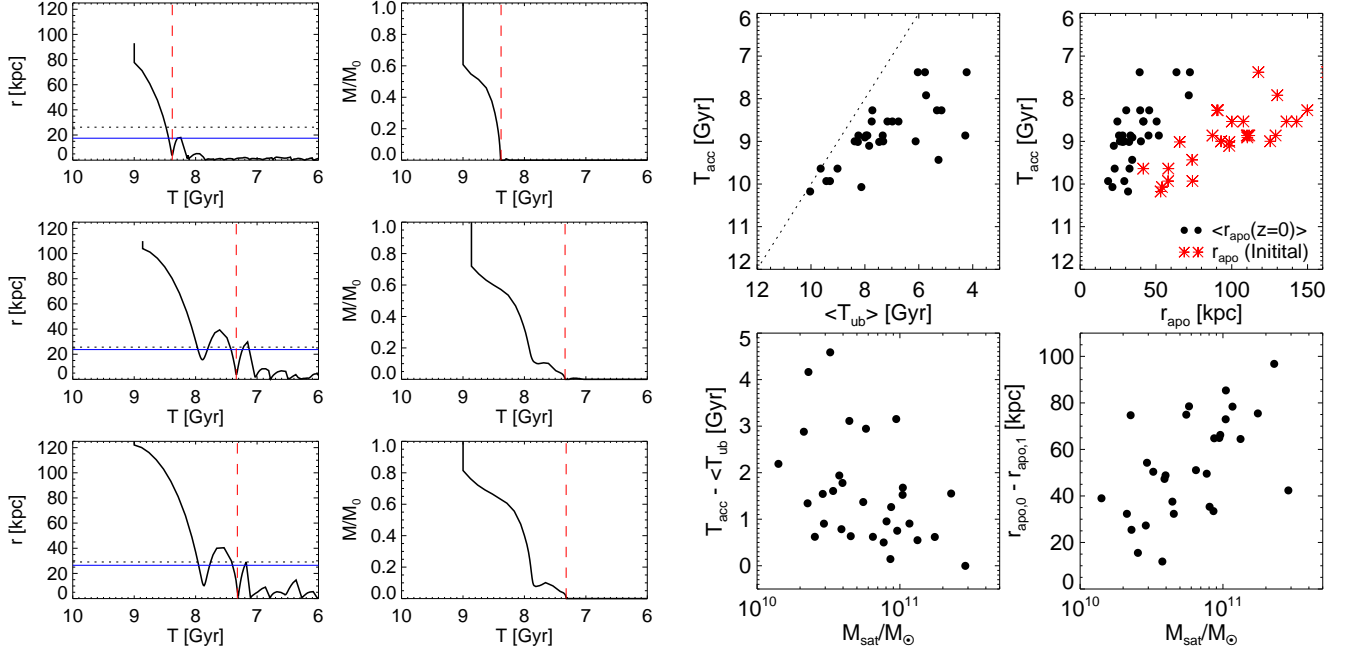


**Figure 7.** *Left hand panels:* Three example satellite orbits from Halo07. The radius (left columns) and mass (right columns) are shown as a function of time. The satellites are followed from their initial apocentre (at accretion) until the satellite is completely disrupted. The dashed red line shows the average time at which the stars belonging to the satellite are stripped. The dotted black lines show the average apocentre of the star particles (at stripping) calculated in Section 4. The solid, blue line shows the estimated break radius of the stripped stellar material. Here, we confirm our deductions in the main text; the break radius is coincident with the apocentre of the satellite near stripping. *Right hand panels:* The top-left panel shows that the average time at which stars are stripped from the satellite is correlated with the time at which the satellite is accreted. The top-right panel shows that the accretion time of a satellite is correlated with both the initial apocentre (red asterisks), and the final apocentre (filled black circles). The bottom two panels show the effect of dynamical friction. We show the orbital time (left panel) and reduction in apocentre (right panel) against satellite mass. More massive satellites are stripped quicker, and have a larger difference between initial and final apocentre.